Desalination and Water Treatment
www.deswater.com
doi: 10.5004/dwt.2020.25771

193 (2020) 159–168
July

Preparation of double-skinned polyamide composite membranes for enhanced forward osmosis desalination

Jingyue Wang, Ziqiang Tong, Baoquan Zhang*

School of Chemical Engineering and Technology, Tianjin University, Tianjin 300350, China, Tel./Fax: +86 13802180732/ +86 2285356517; email: bqzhang@tju.edu.cn (B.Q. Zhang), Tel. +86 15122126161; email: wangjingyue@tju.edu.cn. (J.Y. Wang), Tel. +86 15822472506; email: zqtong@tju.edu.cn (Z.Q. Tong)

Received 22 August 2019; Accepted 27 February 2020

ABSTRACT

Mixed cellulose ester (MCE) porous substrates were first modified by using polyvinyl alcohol (PVA) solutions. Double-skinned polyamide forward osmosis (FO) membranes were fabricated by way of interfacial polymerization on PVA-modified MCE substrates. Field emission scanning electron microscopy was used to observe the morphology change of PVA-modified MCE substrates and the corresponding polyamide active layers. Fourier transform infrared was employed to detect the functional groups of the polyamide layer. Atomic force microscope (AFM) was used to probe membrane topography and surface roughness. The hydrophilicity and mechanical strength of synthesized double-skinned polyamide membranes were, respectively, evaluated by using contact angle and tensile testing experiments. When subjected to the test of FO desalination, the synthesized membrane exhibited satisfactory separation performances with enhanced mechanical strength and long-term stability. Using deionized water as the feed solution and 1 M NaCl aqueous solution as the draw solution, the water flux was 11.32 L m^{-2} h^{-1} and the reverse salt flux was as low as 0.58 g m^{-2} h^{-1}. Compared with available FO membranes in the literature, the synthesized membrane with double-skinned structure should be promising for enhancement of FO performance and long-term operation capacity in practical desalination processes.

Keywords: Forward osmosis; Substrate modification; Double-skinned membrane; Polyamide; Desalination.

1. Introduction

With the growth of the global population and the improvement of living standards, water shortage becomes an increasingly serious problem [1]. Seawater desalination has been considered a promising strategy to solve this issue [2,3]. At present, reverse osmosis (RO) with its relatively mature technology is the most widely used membrane-based separation process for seawater treatment [4,5]. The major challenge that a RO system is facing comes from its high energy consumption because a large external pressure is needed on the feed side to overcome the osmotic pressure [4]. Moreover, severe membrane fouling often occurs in RO operations. In addition to the limitation of plant location and process design, the desalination efficiency of RO systems is only 35%–50%, which not only wastes energy but also produces the concentrated seawater, leading to secondary pollution [6].

Recently, forward osmosis (FO) has begun to be valued as another membrane-based separation technology [7,8], in which the osmotic pressure generated by the concentration difference across the membrane serves as the driving force. Thus, water molecules are spontaneously transported from the feed solution of low concentration to the draw solution

* Corresponding author.

of high concentration while the solute is held in its original place. Finally, the draw solution is concentrated to release pure water to achieve recycling, resulting in a reduction in both operating cost and equipment depreciation [9–11]. This process consumes much less energy than that of RO. A FO membrane is expected to be both stable and durable benefiting from its less susceptible fouling tendency. Due to a series of advantages of FO technologies, such as low cost, easy availability, environmental friendliness, large processing capacity, and independence on high pressure, their application is considered one of the most promising directions for desalination technologies [7,11].

In the development of FO technologies, one of the key issues is to design and fabricate high-quality membranes with acceptable separation performances. Fang et al. [12] prepared polyketone substrates of varied pore size and thickness, and further modified the substrate with metal chlorides. A membrane with polyamide active layer was prepared on the modified substrate, which displayed a good water flux in the FO process. However, the rejection was not ideal due to the inherent defect of the asymmetric membrane structure. Li et al. [13] deposited polyethyleneimine on the polyethersulfone substrate using layer-by-layer assembly and covered with polyacrylic acid to obtain a composite polyethersulfone FO membrane. The membrane mitigated the effects of internal concentration polarization (ICP) and fouling, however, the rejection was not satisfactory and the reverse salt flux was high. Obviously, an active layer with high hydrophilicity, for instance, a polyamide layer (PA), ought to be used [14,15]. Yan et al. [16] prepared a partially reduced freestanding graphene oxide (GO) membrane to lower the ICP effect and avoid its swelling in water. However, the mechanical strength of freestanding GO membranes was weak that could be a serious problem in actual separation processes. Yang et al. [17] fabricated a reduced GO laminate layer covered by dopamine. It exhibited a high flux of water at the very beginning, but the flux declined quickly with time due to membrane fouling. Therefore, antifouling does matter to the fabrication and application of FO membranes.

In general, a high-quality FO membrane should have an ideal water flux and a high rejection of the solute together with satisfactory mechanical strength and stability [18,19]. Unfortunately, the water flux in the FO process is usually much lower than the theoretical expectation due to the existence of serious ICP during operation. The ICP, generated by a concentration gradient inside the porous substrate, would cause a significant decrease in osmotic pressure difference so that the water flux could be reduced by up to 99.9% [9,11,14]. Currently, ultrafiltration or nanofiltration membranes are used as porous substrates due to their high mechanical strength and easy availability. The ICP effect within these substrates cannot be ignored due to the existence of tortuous passages with small apertures [20,21]. Therefore, it would be more appropriate to use microfiltration substrates with relatively large pores to lower the ICP. Obviously, the modification of these substrates, as compensation, is necessary to improve their mechanical strengths and durability. On the other hand, the prepared FO membranes are usually asymmetric. The use of porous substrates makes a remarkable ICP always exist either in the mode of active layer facing the feed solution (AL-FS) or in the mode of active layer facing the draw solution (AL-DS). Once the contaminants enter the pores of a microfiltration substrate, its porosity is lowered and the pore bending factor is increased, resulting in a heavier ICP with a further reduction in water flux [21]. Based on the above analysis, the FO membrane with a double-skinned structure would be beneficial. To date, the double-skinned membrane has been applied in the treatment of organic wastewaters with good anti-contamination properties and ICP reduction [22–24]. However, the resistance to water permeation through the doubled membrane would increase, leading to a serious decrease in water flux [25].

In this work, double-skinned FO membranes are to be prepared. PA is chosen as the active layer, while the mixed cellulose ester (MCE) microfiltration membrane with a pore size of 0.22 μm is selected as the substrate. Polyvinyl alcohol (PVA) is used to modified MCE substrate to increase its hydrophilicity and mechanical strength, and a crosslinking reaction by using glutaraldehyde (GA) is carried out to stabilize PVA chains attached on MCE substrate. It could be expected that the synthesized double-skinned PA membrane on PVA-modified MCE in this study would exhibit a satisfactory desalination performance with a good antipollution property and long-term stability. Up to now, there are no relevant results available in open publications.

2. Materials and methods

2.1. Materials

MCE (50 mm in diameter, 0.22 μm aperture) provided by Tianjin Shengze Technology Co., Ltd., China, was used as the substrate. PVA (98.0–99.0 mol %) and glutaraldehyde (GA, 50%) were purchased from Shanghai Aladdin Bio-Chem Technology Co., Ltd, China. Hydrochloric acid (HCl, 36.0%–38.0%) and acetone (99%) were obtained from Tianjin Damao Chemical Co., Ltd., China. 1,3-Phenylenediamine (MPD, 99.5%) was purchased from Nanjing Shengbicheng Chemical Technology Co., Ltd., China. Trimesoyl chloride (TMC, 98%) was supplied by Tianjin Heowns Bio-Chem Technology Co., Ltd., China. *N*-hexane (98%) was purchased from Tianjin Fuchen Chemical Technology Co., Ltd., China. Sodium chloride (NaCl, 99.5%) was purchased from Tianjin Jiangtian Chemical Technology Co., Ltd., China. Deionized water (DI H_2O) was produced on a water purifier (Ulupure-II-10 T, Chengdu Ultrapure Technology Co., Ltd., China) with a resistivity of 18.25 MΩ cm.

2.2. Modification of MCE substrates

The MCE substrate was modified by using a PVA solution to increase its hydrophilicity and mechanical strength [26,27]. First, 1, 2, and 4 wt.% PVA solutions were, respectively, prepared under a water bath at 95°C. Thereafter, the substrate was immersed in a PVA solution at 60°C overnight. In the following step, the excess PVA solution was removed, and the sample was dried in an oven at 100°C for 10 min. To achieve the crosslinking of PVA chains, the dried substrate was put into a glutaraldehyde solution (50 mM L^{-1} GA, 20 mM L^{-1} HCl, acetone to water volume ratio of 1:3)

at room temperature for 30 min. After wiping off the excess GA solution, the modified MCE substrate was dried at 100°C for 10 min, and then stored for further use. The substrates modified with PVA solutions were named as 1PVA-MCE, 2PVA-MCE, and 4PVA-MCE, respectively. The numbers 1, 2, and 4 were referred to the corresponding concentration of the used PVA solution.

2.3. Preparation of double-skinned PA membranes

The modified MCE substrate was washed in DI water at first and then soaked in a 3 wt.% MPD solution (acetone to water volume ratio of 1:2) for 5 min. After removing the excess liquid, it was immersed in a 0.15 wt.% TMC/*n*-hexane solution for 2 min. The membrane was taken out of the solution after the polymerization reaction was completed and dried at room temperature prior to use. The prepared double-skinned PA membranes were named as PA-1PVA-MCE, PA-2PVA-MCE, and PA-4PVA-MCE based on the used substrates, respectively. In the same way, this process was repeated to obtain the double-skinned PA membrane adhered to an unmodified MCE substrate named PA-MCE.

In addition, single-skinned PA FO membranes were also prepared for comparison. After washed with DI water, the modified MCE substrate was fixed on a ring-shaped device (Fig. S1, Supporting Information) with only one side opening upwards, and was evenly coated with 2 wt.% MPD solution for 5 min. The sample was carefully dismounted from the device to remove excess liquid. Then, it was fixed on the device once again. 0.15 wt.% TMC solution was quickly applied to the side with MPD, and the reaction was performed for 2 min, followed by drying at room temperature prior to use. The single-skinned PA membrane was named by adding a "S" in front of the corresponding double-skinned PA membrane, for example, S-PA-2PVA-MCE.

2.4. Characterization

Scanning electron microscopy (SEM) images were recorded on a Hitachi S-4800 SEM at an acceleration voltage of 5 kV. Tension tests were performed on a mini-type in-situ tensile testing system (IBTC-300s, CARE Measurement and Control Co., Ltd.) with respect to MCE substrates or double-skinned PA membranes sized at 2 cm × 1 cm to obtain a stress-strain curve. Tests were measured at the strain rate of 0.003 s^{-1} and determined with a non-contact displacement detecting system to gain precise results [28]. Apparent contact angles were tested at room temperature using a contact angle goniometer (JC2000D2M Contact Angle Meter). Membrane topography and roughness were probed by an atomic force microscope (AFM, NSG10) in tapping mode. Fourier transform infrared (FT-IR) spectrum was measured with KBr media using a Thermo Scientific Nicolet 6700 FT-IR spectrometer.

2.5. FO performance measurements

The water flux and salt rejection of synthesized membranes were measured on a laboratory-scale H-shaped forward osmosis device (Fig. 1). The two compartments were connected via the two attached circular tubes of the same diameter, and the area of the sandwiched membrane was 1.767 cm^2. The feed side was DI water and the draw side was sodium chloride (NaCl) aqueous solution, which were, respectively, added to the two compartments before measurements. Magnetic stirring was used to eliminate external concentration polarization. The conductivity of the feed solution was monitored using a conductivity meter. Prior to actual operations, a standard curve was measured to give the conductivity-concentration relation. For the synthesized double-skinned membranes PA-MCE, PA-1PVA-MCE, PA-2PVA-MCE, and PA-4PVA-MCE, the feed solution was DI water and the draw solution was 1 M NaCl aqueous solution. To test the effect of concentration gradients, the feed solution was still DI water while the draw solutions were 0.5, 1, 1.5, and 2.0 M NaCl aqueous solutions, respectively. Since the prepared double-skinned FO membrane possessed a symmetric structure, it was no need to distinguish AL-DS and AL-FS modes.

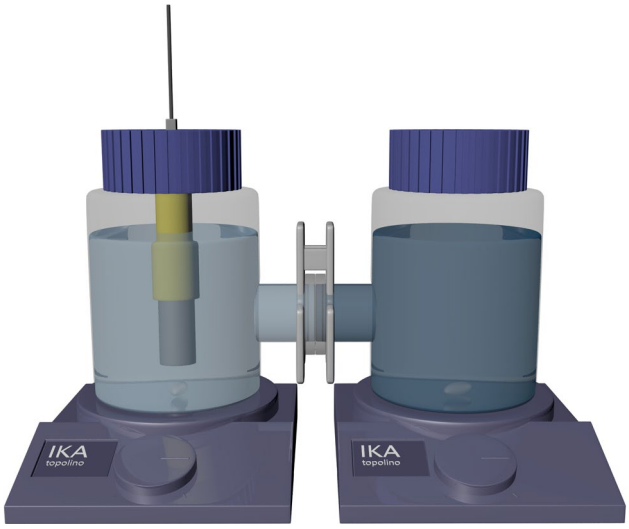

Fig. 1. H-shaped forward osmosis device.

In addition, single-skinned FO membranes were checked using the same feed and draw solutions to analyze the effect of membrane structure on desalination performances. The tests were performed under both AL-DS and AL-FS modes.

The water flux was calculated by using:

$$J_w = \frac{-\Delta V_{\text{feed}}}{\left(A_m \times \Delta t\right)} \tag{1}$$

where J_w (L m^{-2} h^{-1}, LMH) is the water flux, A_m the effective membrane area, ΔV_{feed} the feed liquid volume change, and Δt the test time.

The reverse salt flux could be calculated according to:

$$J_s = \frac{-\Delta C_{t,\text{feed}} V_{t,\text{feed}}}{\left(A_m \times \Delta t\right)} \tag{2}$$

where J_s (g m^{-2} h^{-1}, gMH) is the reverse salt flux, $\Delta C_{t,\text{feed}}$ the feed solution concentration change over the time period Δt, and $\Delta V_{t,\text{feed}}$ the feed volume change after

testing time. The test under the same operation condition was measured at least three times and averaged.

2.6. Stability assessments

To investigate the effect of the double-skinned structure on membrane stability, the consecutive FO experiments were performed for both double-skinned and single-skinned membranes. The feed solution was 3.5 wt.% or 2 M NaCl aqueous solution was used as the draw solution. The experiment was performed for 24 h, and the volume change of the feed solution was measured every three hours to calculate the water flux.

3. Results and discussion

3.1. Effect of PVA modification on substrate and membrane morphologies

Fig. 2a gives the network structure of MCE substrates, the voidage of which is very high. After modification, the connected fibers in the network structure are reinforced due to PVA deposition (Fig. 2b). Nevertheless, the observed voidage is pretty high for either the MCE substrate itself or its modified counterpart. The double-skinned PA membrane on an unmodified MCE substrate (PA-MCE) is displayed in Fig. 2c, and its magnified image is given in Fig. 2d. The outer surface of PA-MCE demonstrates a regular ridge and valley morphology. However, the synthesized double-skinned PA membrane on the modified MCE substrate (PA-2PVA-MCE) exhibits a concentrated ridge and valley structure (Fig. 2e). This should be attributed to the modification of the MCE substrate using PVA. When the modified MCE substrate was immersed in the MPD solution, MPD molecules would interact with PVA molecules by way of hydrogen bonding. This interaction would slow the diffusion of MPD molecules when the modified MCE substrate is immersed in the TMC/*n*-hexane solution, resulting in the polymerization on uneven surfaces and the formation of the undulating surface structure (Figs. 2e and f) [29]. Based on the visual observation (Fig. 2f), the active PA layer of PA-2PVA-MCE is ca. 200 nm thick. It should be noted that this extremely undulating structure makes the effective membrane area substantially increased. As a result, higher water fluxes could be expected for this double-skinned FO membrane with the dense undulating surface structure.

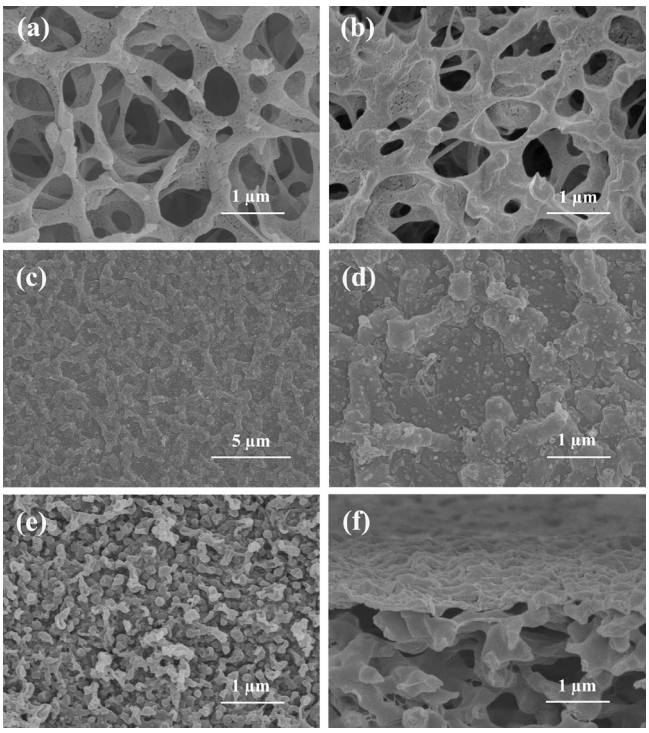

Fig. 2. SEM images of MCE (a), 2PVA-MCE (b), PA-MCE (c), with its magnified image (d), and PA-2PVA-MCE (e) with its cross-sectional image (f).

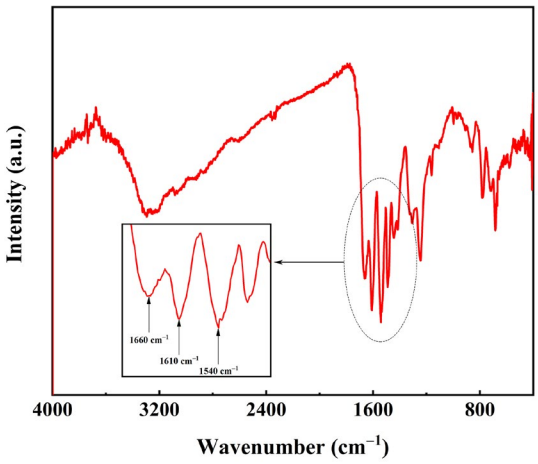

Fig. 3. FT-IR spectrum of the PA active layer from PA-2PVA-MCE membrane.

3.2. FT-IR analysis

To prove the successful preparation of the double-skinned PA membrane on the modified MCE substrate, the active PA layer of PA-2PVA-MCE was peeled off, and subjected to infrared spectroscopy. As shown in Fig. 3, the peaks at 1,660; 1,610; and 1,540 cm^{-1} represent C=O, N–H, and C–N bonds, respectively. These three peaks could indicate that the active PA layer has been successfully covered on the PVA modified MCE substrate.

3.3. Effect of PVA modification on membrane surface roughness

The AFM images show the difference in roughness for PA-MCE and PA-2PVA-MCE (Fig. 4). PA-2PVA-MCE has got a larger average roughness (159 nm) than that of PA-MCE (134 nm), indicating the addition of PVA made the active layer rougher. In other words, PVA modification increased the effective surface area of PA active layer, which should be conducive to the enhancement of water permeation.

3.4. Effect of PVA modification on hydrophilicity

The modification of the MCE substrate should lead to a change in its surface hydrophilicity due to PVA deposition on MCE fibers (Fig. 2b). As demonstrated above, the

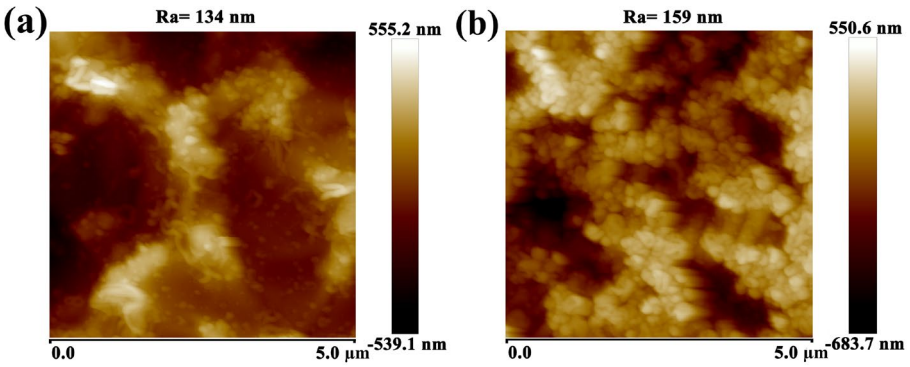

Fig. 4. AFM images of PA-MCE (a) and PA-2PVA-MCE (b).

existence of PVA molecules on modified MCE substrates made the polymerization on uneven surfaces, resulting in the formation of undulating PA top-layers with changes in surface hydrophilicity for double-skinned PA membranes.

The dynamic contact angle tests were carried out on the surfaces of MCE, 2PVA-MCE, PA-MCE, and PA-2PVA-MCE. As summarized in Fig. 5, the modification of the MCE substrate with PVA leads to an increase in surface hydrophilicity for both the substrate itself and the active PA layer on the substrate. At the very beginning, the contact angle of the MCE substrate is ca. 103°, exhibiting poor hydrophilicity. However, the contact angle of the modified substrate (2PVA-MCE) is reduced to ca. 88°. The reduction of the contact angle is further enlarged to ca. 30° after 20 s, suggesting the improvement in surface hydrophilicity for the modified MCE substrate.

It should be noted that the initial contact angle of PA-MCE is slightly lower than that of PA-2PVA-MCE due to the difference in surface roughness. However, the contact angle of PA-2PVA-MCE is reduced faster than that of PA-MCE, the value of which could reach to ca. 33°. Obviously, the improvement in surface hydrophilicity via the modification of MCE substrates should be conducive to acquiring high water fluxes for FO membranes.

3.5. Variations of mechanical strengths

For MCE substrates, the effect of PVA modification on the mechanical properties is given in Fig. 6a. Based on the measured stress-strain relations, the MCE substrate can bear a tensile strength of 7.61 MPa with 3.41% elongation at break. After the modification with PVA, the tensile strength of 2PVA-MCE can reach to 9.16 MPa with 3.7% elongation at break, leading to a nearly 20% increase in tensile strength at break. As for the double-skinned PA membrane on the MCE substrate, the substrate modification with PVA possesses a more pronounced effect on its mechanical properties as observed in Fig. 6b. The membrane PA-2PVA-MCE could withstand a tensile strength of 12.31 MPa with 9.80% elongation at break representing a 37% increase in tensile strength at break compared with the membrane PA-MCE. Therefore, the PVA modification could effectively improve the mechanical properties of MCE substrates and double-skinned PA membranes, which should be conducive to keeping their long-term stabilities in practical operations.

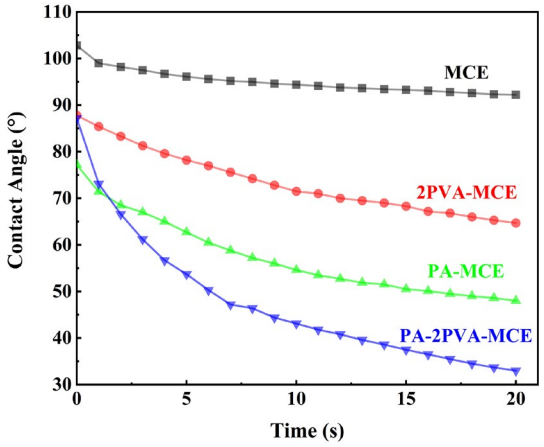

Fig. 5. Variations of contact angles with time for MCE, 2PVA-MCE, PA-MCE, and PA-2PVA-MCE.

3.6. FO performances of double-skinned PA membranes

The FO performances of synthesized double-skinned PA membranes were tested, including PA-MCE, PA-1PVA-MCE, PA-2PVA-MCE, and PA-4PVA-MCE. All experiments were conducted with DI water as the feed solution and 1 M NaCl aqueous solution as the draw solution. Since the used PA membranes all possess symmetric double-skinned structures, it is not necessary to distinguish the direction to which the active PA layer faces.

As shown in Fig. 7a, the water flux of PA-MCE is ca. 5.66 LMH with a reverse salt flux of ca. 0.20 g MH. For the double-skinned PA membranes on modified MCE substrates, the water flux increases with the PVA concentration in the modification of MCE substrates. These results might be explained by the increase in surface hydrophilicity and effective area for double-skinned PA membranes on modified MCE substrates. However, the variation of reverse salt flux with PVA concentration is not monotonic. The ratio of J_s/J_w, as a key parameter for evaluation of FO membranes, is only 0.05 g L^{-1} for PA-2PVA-MCE, which is the lowest one in the synthesized FO membranes (Fig. 7b). The optimum PVA concentration in the modification of MCE substrates should be 2 wt.% based on the ratio of J_s/J_w.

Based on the above results, the membrane PA-2PVA-MCE was selected to study the effect of concentration

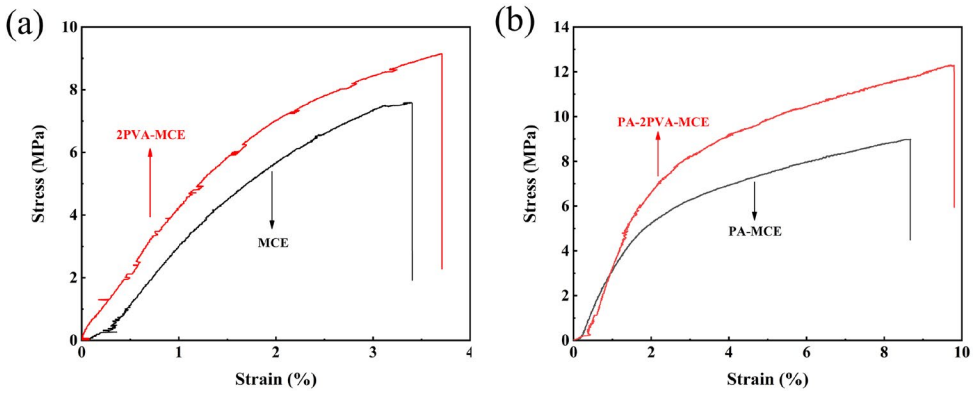

Fig. 6. Effects of PVA modification on tensile strengths for MCE substrate (a) and double-skinned PA membrane (b).

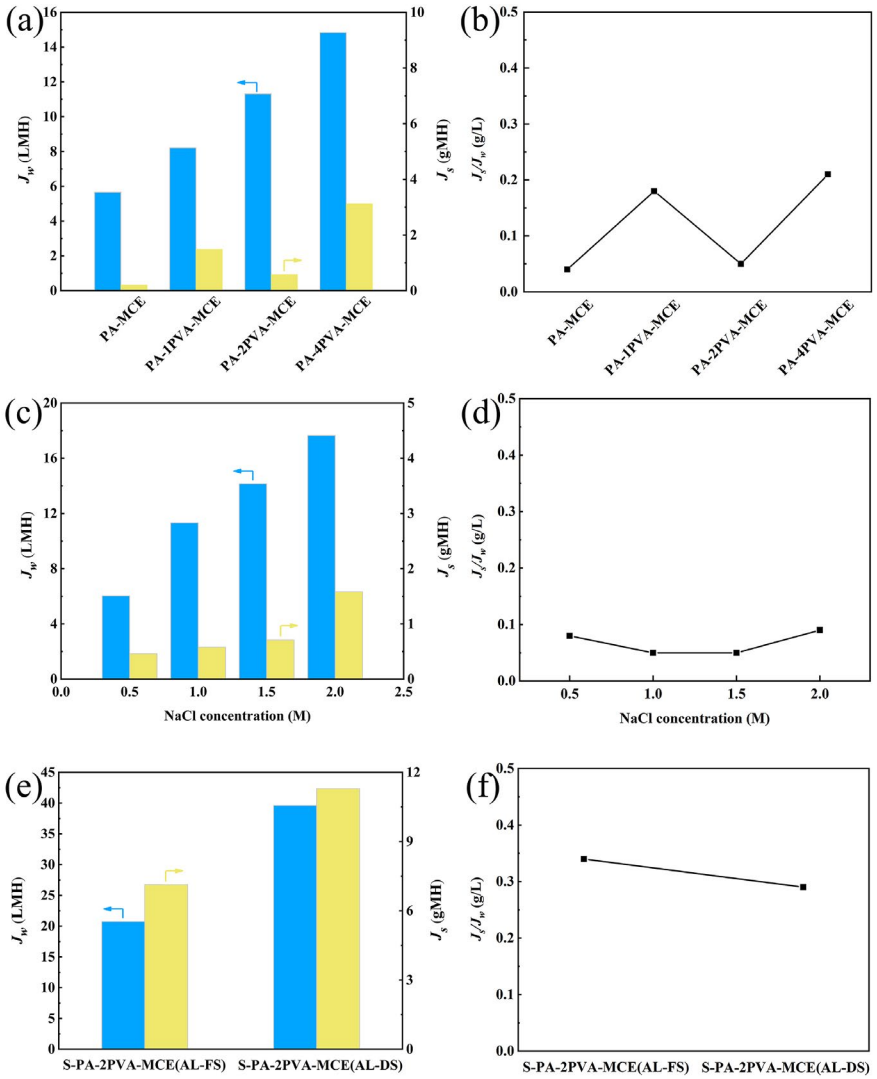

Fig. 7. (a) FO performances for PA-MCE, PA-1PVA-MCE, PA-2PVA-MCE, and PA-4PVA-MCE with 1 M NaCl aqueous solution as the draw solution. (b) J_s/J_w for PA-MCE, PA-1PVA-MCE, PA-2PVA-MCE, and PA-4PVA-MCE with 1 M NaCl aqueous solution as the draw solution. (c) FO performances for PA-2PVA-MCE under different NaCl concentrations in the draw solution. (d) J_s/J_w for PA-2PVA-MCE under different NaCl concentrations in the draw solution. (e) FO performances for S-PA-2PVA-MCE under both AL-FS and AL-DS modes with 2 M NaCl aqueous solution as the draw solution. (f) J_s/J_w values for S-PA-2PVA-MCE under both AL-FS and AL-DS modes with 2 M NaCl aqueous solution as the draw solution.

gradients in the draw solution. As shown in Fig. 7c, the feed solution is DI water while the draw solutions are 0.5, 1, 1.5, and 2 M NaCl aqueous solutions, respectively. The water flux together with the reverse salt flux is going up when the NaCl concentration in the draw solution increases, owing to the increase in the driving force. When the draw solution concentration is varied from 0.5 to 1 M, the water flux is almost doubled from 6.04 to 11.32 LMH. As the draw solution concentration is shifted from 1 to 2 M, the water flux is only increased by 0.6 times, suggesting that the FO process is not affected by the ICP at low concentration in the draw solution whereas it is influenced by the ICP when the NaCl concentration is higher. Therefore, under a low or medium concentration in the draw solution, no effect of ICP in the double-skinned membrane PA-2PVA-MCE could be observed. By using the 1 M NaCl aqueous solution as the draw solution, 11.32 LMH water flux, and extremely low reverse salt flux (0.58 g MH) have been achieved. J_s/J_w remains relatively stable throughout the process (Fig. 7d).

For comparison, the single-skinned PA membrane S-PA-PVA2-MCE was also tested under both AL-DS and AL-FS modes, which was further compared with the corresponding double-skinned PA membrane PA-PVA2-MCE. The experiments were conducted with DI water as the feed solution and 2 M NaCl aqueous solution as the draw solution. By comparison to PA-PVA2-MCE, the water flux of S-PA-PVA2-MCE under both modes was going up accompanied by a substantial increase of reverse salt flux (Fig. 6e), resulting in at least two-fold increase in J_s/J_w for S-PA-PVA2-MCE (Fig. 6f). Indeed, the double-skinned structure lowered the membrane permeability due to its increased mass transfer resistance, however, it can give rise to a substantially improved rejection performance for the FO process.

As shown in Table 1, the FO performance of the synthesized double-skinned membrane is listed and compared with those of available membranes in the literature. Due to its double-skinned structure, the water flux of the membrane PA-2PVA-MCE synthesized in this study is lower than those of listed FO membranes under the same operation condition, however, its rejection effect is much enhanced with the lowest J_s/J_w. The membrane PA-2PVA-MCE possesses a comparable water flux and a high rejection, which would be advantageous to seawater desalination to achieve high separation efficiencies.

3.7. Membrane stability

To check the stability of synthesized double-skinned PA membranes, both PA-2PVA-MCE and S-PA-PVA2-MCE (AL-DS) were chosen in the test. In order to simulate the real seawater desalination system, 3.5 wt.% NaCl aqueous solution (about 0.6 M) was selected as the feed solution and 2 M NaCl aqueous solution as the draw solution. The water flux was recorded every three hours in the FO process. As presented in Fig. 8, the water flux of PA-PVA2-MCE could remain stable over the whole process with the mean value of 12.17 LMH, proving that the fouling within the membrane could be negligible. With respect to

Table 1
Comparison with FO performances of available FO membranes

FO membrane	Draw solution (M NaCl)	Orientation mode	J_w (LMH)	J_s (gMH)	J_s/J_w (g L^{-1})	Reference
GPA-0.45[a]	1	AL-DS	26.72	3.86	0.14	[3]
		AL-FS	17.24	3.73	0.22	
F-CGO[b]	1	–	18.80	5.84	0.31	[16]
GO-MPD/TMC[c]	1	AL-DS	20.80	3.40	0.16	[30]
		AL-FS	17.29	2.12	0.12	
M4[d]	1	AL-DS	24.00	2.80	0.12	[31]
TFN-2[e]	1	AL-DS	23.60	6.9	0.29	[32]
		AL-FS	13.40	6.2	0.46	
TFN 0.05[f]	0.5	AL-DS	44.02	7.41	0.17	[33]
		AL-FS	29.88	4.35	0.15	
Single skin PA-2PVA-MCE	2	AL-FS	20.75	7.13	0.34	This work
PA-2PVA-MCE	2	AL-DS	39.62	11.29	0.29	
	1	–	11.32	0.58	0.05	
	2	–	17.66	1.58	0.09	

The feed solution is DI water.
[a]Polyamide active layer was formed on the nylon substrate containing GO/MWCNT layer.
[b]Freestanding graphene-based laminar membrane by thermally-induced chemical cross-linking.
[c]GO-based MPD/TMC crosslinking membranes by pressure-assisted self-assembly technique.
[d]Polyamide active layer was formed on polysulfone substrate and conducted surface mineralization modification by depositing silver chloride (AgCl) particles on the surfaces.
[e]PSf substrates with varied LDH/GO loadings.
[f]Hydrophilic/hydrophobic interpenetrating network composite nanofibers (HH-IPN-CNF) as substrate were prepared by electrospinning technology, and the PA active layer was formed by interfacial polymerization using MPD/GO/TMC.

Table 2
Comparison with FO performances of available FO membranes

FO membranes	Feed solution	Draw solution	$J_{w,0h}$ (LMH)	$J_{w,6h}$ (LMH)	$J_{w,12h}$ (LMH)	$J_{w,18h}$ (LMH)	Reference
pDA-rGO[a]	DI water	0.6 M NaCl	54.55	38.18	23.18	–	[17]
GO-TMC[b]	DI water	2 M NaCl	10.50	5.25	–	–	[30]
GO-TMC/MPD[c]	DI water	2 M NaCl	20.80	20.70	–	–	
M4[d]	10 mM NaCl and 200 mg L^{-1} BSA	0.5-1.5 M NaCl	24.00	18.00	–	–	[31]
MTFC[e]	1,000 mg L^{-1} phenol	1 M NaCl	11.40	8.60	–	–	[34]
TFN[f]	Municipal water	1 M NaCl	28.00	24.86	22.29	21.43	[35]
S-PA-2PVA-MCE	3.5 wt.% NaCl	2 M NaCl	16.83	15.45	12.96	11.24	This work
PA-2PVA-MCE	3.5 wt.% NaCl	2 M NaCl	13.39	12.51	11.13	12.32	

[a]rGO membrane coated by pDA.
[b,c]GO-based TMC and MPD/TMC crosslinking membranes by using the pressure-assisted self-assembly technique.
[d]Membrane fabricated using CuBDC-NS as the nanofiller in the PA active layer.
[e]AgCl mineralized TFC PA membranes.
[f]Polyamide active layer was formed on the polysulfone substrates and conducted surface mineralization modification by depositing AgCl particles on the surfaces.

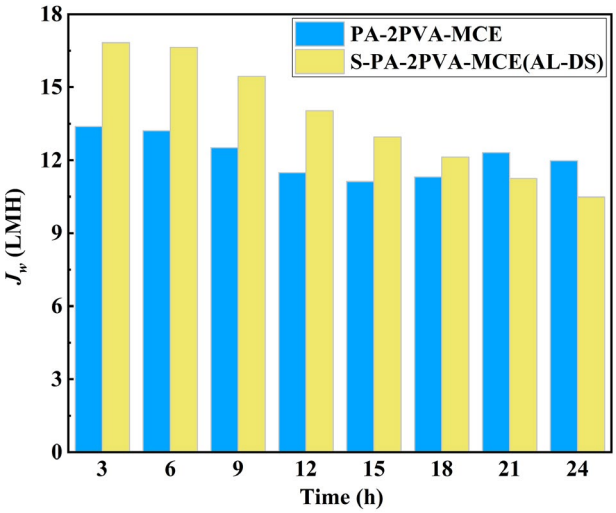

Fig. 8. FO performances of PA-2PVA-MCE and S-PA-2PVA-MCE(AL-DS) in 24 h.

S-PA-PVA2-MCE, the situation was different. The water flux of S-PA-PVA2-MCE was continuously decreased with time, dropping to ca. 60% of its original value in 24 h. Based on these experiments, it can be demonstrated that double-skinned FO membrane prepared in this study could effectively prevent the flux drop caused by membrane fouling and remain long-term stability in practical seawater treatment.

As described above, the FO performances of the membrane PA-2PVA-MCE could keep stable in a long-term operation, the comparison of which with those of reported FO membranes in the literature is shown in Table 2. Although the double-skinned PA-2PVA-MCE membrane has a relatively low water flux at the beginning, it maintains the same over the time of operation. In contrast, the reported FO membranes in the literature do have a higher water flux at the beginning of measurements, but the water flux decreases sharply with time due to membrane fouling. Evidently, the double-skinned FO membranes are conducive to long-term desalination processes due to their excellent anti-pollution behaviors.

4. Conclusions

The MCE substrate was first modified by using PVA solutions with different concentrations, leading to an improvement in hydrophilicity and mechanical strengths. The double-skinned PA membrane was successfully prepared by interfacial polymerization on both sides of the modified MCE substrate. The PVA modification of MCE substrate exhibited a significant effect on the morphology of the PA active layer with an enlarged surface area, at the same time, the mechanical strengths, and hydrophilicity of double-skinned PA membranes were improved accordingly. The synthesized membrane PA-2PVA-MCE displayed a moderate water flux (11.32 LMH) with an extremely low reverse salt flux (0.58 g MH) when the feed solution was pure water and the draw solution was 1 M NaCl aqueous solution. Compared with available FO membranes in the literature, the use of the double-skinned structure in this study effectively reduced ICP and endowed the membrane with excellent anti-fouling ability, leading to a significant improvement in its long-term stability. It was revealed that double-skinned PA membranes on modified substrates could be applied in FO desalination with acceptable water flux, excellent salt rejection, improved mechanical strength, and long-term stability. Moreover, a new method was supplied to design high-performance FO membranes for application in wastewater treatment and water purification processes.

Acknowledgment

We are grateful for the financial support from the National Natural Science Foundation of China (Grant No. 21136008).

References

[1] A. Subramani, J.D. Jacangelo, Emerging desalination technologies for water treatment: a critical review, Water Res., 75 (2015) 164–187.

[2] Q.Y. Wu, X.Y. Xing, Y. Yu, Novel thin film composite membranes supported by cellulose triacetate porous substrates for high-performance forward osmosis, Polymer, 153 (2018) 150–160.

[3] W. Zhao, H.Y. Liu, Y. Liu, M.P. Jian, L. Gao, H.T. Wang, X.W. Zhang, Thin-film nanocomposite forward-osmosis membranes on hydrophilic microfiltration support with an intermediate layer of graphene oxide and multiwall carbon nanotube, ACS Appl. Mater. Interfaces, 10 (2018) 34464–34474.

[4] L.F. Greenlee, D.F. Lawler, B.D. Freeman, B. Marrot, P. Moulin, Reverse osmosis desalination: water sources, technology, and today's challenges, Water Res., 43 (2009) 2317–2348.

[5] R.W. Baker, Membrane Technology and Applications, 3rd ed., John Wiley and Sons Ltd., Chichester, 2012.

[6] T.Y. Cath, A.E. Childress, E. Menachem, Forward osmosis: principles, applications, and recent developments, J. Membr. Sci., 281 (2006) 70–87.

[7] B. Kim, G. Gwak, S. Hong, Review on methodology for determining forward osmosis (FO) membrane characteristics: water permeability (A), solute permeability (B), and structural parameter (S), Desalination, 422 (2017) 5–16.

[8] Q.V. Ly, Y.X. Hu, J.X. Li, J.W. Cho, J. Hur, Characteristics and influencing factors of organic fouling in forward osmosis operation for wastewater applications: a comprehensive review, Environ. Int., 129 (2019) 164–184.

[9] S.F. Zhao, L.D. Zou, C.Y.Y. Tang, D. Mulcahy, Recent developments in forward osmosis: opportunities and challenges, J. Membr. Sci., 396 (2012) 1–21.

[10] L. Chekli, S. Phuntsho, J.E. Kim, J. Kim, J.Y. Choi, J.S. Choi, S. Kim, J.H. Kim, S. Hong, J. Sohn, H.K. Shon, A comprehensive review of hybrid forward osmosis systems: performance, applications and future prospects, J. Membr. Sci., 497 (2016) 430–449.

[11] S. Phuntsho, H.Y. Shon, T. Zhang, R. Surampalli, Chapter 1 – Introduction: Role of Membrane Science and Technology and Forward Osmosis Processes, H.K. Shon, S. Phuntsho, T.C. Zhang, R.Y. Surampalli, Eds., Forward Osmosis: Fundamentals and Applications, American Society of Civil Engineers, Reston, Virginia, 2015, pp. 1–14.

[12] L.F. Fang, L. Cheng, S. Jeon, S.Y. Wang, T. Takahashi, H. Matsuyama, Effect of the supporting layer structures on antifouling properties of forward osmosis membranes in AL-DS mode, J. Membr. Sci., 552 (2018) 265–273.

[13] M.N. Li, X.F. Sun, L. Wang, S.Y. Wang, M.Z. Afzal, C. Song, S.G. Wang, Forward osmosis membranes modified with laminar MoS_2 nanosheet to improve desalination performance and antifouling properties, Desalination, 436 (2018) 107–113.

[14] W.J. Lau, S. Gray, T. Matsuura, D. Emadzadeh, J.P. Chen, A.F. Ismail, A review on polyamide thin film nanocomposite (TFN) membranes: history, applications, challenges and approaches, Water Res., 80 (2015) 306–324.

[15] L. Shen, W.S. Hung, J. Zuo, X. Zhang, J.Y. Lai, Y. Wang, High-performance thin-film composite polyamide membranes developed with green ultrasound-assisted interfacial polymerization, J. Membr. Sci., 570 (2019) 112–119.

[16] F. Yan, C.H. Yu, B.W. Zhang, T. Zou, H.W. Zhao, J.Y. Li, Preparation of freestanding graphene-based laminar membrane for clean-water intake via forward osmosis process, RSC Adv., 7 (2017) 1326–1335.

[17] E. Yang, C.M. Kim, J.H. Song, H. Ki, M.H. Ham, I.S. Kim, Enhanced desalination performance of forward osmosis membranes based on reduced graphene oxide laminates coated with hydrophilic polydopamine, Carbon, 117 (2017) 293–300.

[18] W.X. Xu, Q.C. Ge, Novel functionalized forward osmosis (FO) membranes for FO desalination: improved process performance and fouling resistance, J. Membr. Sci., 555 (2018) 507–516.

[19] X.Y. Zhang, S.S. Gao, T.Y. Tian, S.J. Shan, R. Takagi, F.Y. Cui, L.M. Bai, H. Matsuyama, Investigation of cleaning strategies for an antifouling thin-film composite forward osmosis membrane for treatment of polymer-flooding produced water, Ind. Eng. Chem. Res., 58 (2019) 994–1003.

[20] H.Q. Liang, W.S. Hung, H.H. Yu, C.C. Hu, K.R. Lee, J.Y. Lai, Z.K. Xu, Forward osmosis membranes with unprecedented water flux, J. Membr. Sci., 529 (2017) 47–54.

[21] H.Y. Liu, H.T. Wang, X.W. Zhang, Facile fabrication of freestanding ultrathin reduced graphene oxide membranes for water purification, Adv. Mater., 27 (2015) 249–254.

[22] P.H.H. Duong, T.S. Chung, S. Wei, L. Irish, Highly permeable double-skinned forward osmosis membranes for anti-fouling in the emulsified oil–water separation process, Environ. Sci. Technol., 48 (2014) 4537–4545.

[23] L. Luo, Z.Z. Zhou, T.S. Chung, M. Weber, C. Staudt, C. Maletzko, Experiments and modeling of boric acid permeation through double-skinned forward osmosis membranes, Environ. Sci. Technol., 50 (2016) 7696–7705.

[24] D.Y.F. Ng, B. Wu, Y.F. Chen, Z.L. Dong, R. Wang, A novel thin film composite hollow fiber osmotic membrane with one-step prepared dual-layer substrate for sludge thickening, J. Membr. Sci., 575 (2019) 98–108.

[25] Z.Z. Zhou, J.Y. Lee, Evaluating the viability of double-skin thin film composite membranes in forward osmosis processes, J. Membr. Sci., 502 (2016) 65–75.

[26] M.J. Park, R.R. Gonzales, A. Abdel-Wahab, S. Phuntsho, H.K. Shon, Hydrophilic polyvinyl alcohol coating on hydrophobic electrospun nanofiber membrane for high performance thin film composite forward osmosis membrane, Desalination, 426 (2018) 50–59.

[27] H.M. Song, L.J. Zhu, Z.X. Zeng, Q.J. Xue, High performance forward osmosis cellulose acetate (CA) membrane modified by polyvinyl alcohol and polydopamine, J. Polym. Res., 25 (2018) 159.

[28] Q. Lin, Z. Liu, L. Wang, X. Chen, S.W. Shi, Fracture property of Nafion XL composite membrane determined by R-curve method, J. Power Sources, 398 (2018) 34–41.

[29] Z. Tan, S.F. Chen, X.S. Peng, L. Zhang, C.J. Gao, Polyamide membranes with nanoscale Turing structures for water purification, Science, 360 (2018) 518–521.

[30] W.S. Hung, Y.H. Chiao, A. Sengupta, Y.W. Lin, A.R. Wickramasinghe, C.C. Hu, H.A. Tsai, K.R. Lee, J.Y. Lai, Tuning the interlayer spacing of forward osmosis membranes based on ultrathin graphene oxide to achieve desired performance, Carbon, 142 (2019) 337–345.

[31] H.Y. Jin, F. Rivers, H.D. Yin, T.M. Lai, P. Cay-Durgun, A. Khosravi, M.L. Ling, P. Yu, Synthesis of AgCl mineralized thin film composite polyamide membranes to enhance performance and antifouling properties in forward osmosis, Ind. Eng. Chem. Res., 56 (2017) 1064–1073.

[32] P. Lu, S. Liang, T. Zhou, X. Mei, Y. Zhang, C. Zhang, A. Umar, Q. Wang, Layered double hydroxide/graphene oxide hybrid incorporated polysulfone substrate for thin-film nanocomposite forward osmosis membranes, RSC Adv., 6 (2016) 56599–56609.

[33] E.L. Tian, X.Z. Wang, X. Wang, Y.W. Ren, Y.T. Zhao, X.C. An, Preparation and characterization of thin-film nanocomposite membrane with high flux and antibacterial performance for forward osmosis, Ind. Eng. Chem. Res., 58 (2019) 897–907.

[34] Y.B. Huang, P. Cay-Durgun, T.M. Lai, P. Yu, M.L. Lind, Phenol removal from water by polyamide and AgCl mineralized thin-film composite forward osmosis membranes, Ind. Eng. Chem. Res., 57 (2018) 7021–7029.

[35] R.B. Dai, X.R. Zhang, M.X. Liu, Z.C. Wu, Z.W. Wang, Porous metal organic framework CuBDC nanosheet incorporated thin-film nanocomposite membrane for high-performance forward osmosis, J. Membr. Sci., 573 (2019) 46–54.

Supplementary information

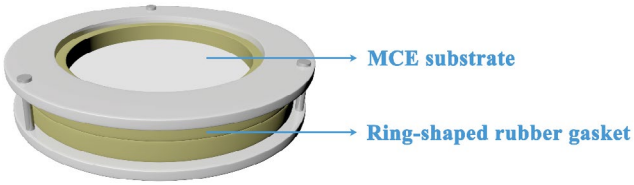

Fig. S1. Ring-shaped device for preparing single skin PA FO membrane.